IEEE Access
Multidisciplinary | Rapid Review | Open Access Journal

IEEE VEHICULAR TECHNOLOGY SOCIETY SECTION

Received 18 August 2022, accepted 24 September 2022, date of publication 26 September 2022, date of current version 4 October 2022.

Digital Object Identifier 10.1109/ACCESS.2022.3210123

RESEARCH ARTICLE

State-Feedback-Critical Super Twisting Sliding Mode Control for a Half-Car Suspension System

DUC GIAP NGUYEN[1], KYOUNGTAE JI[1], (Graduate Student Member, IEEE), TAM W. NGUYEN[2], (Member, IEEE), AND KYOUNGSEOK HAN[1], (Member, IEEE)

[1]School of Mechanical Engineering, Kyungpook National University, Daegu 41566, South Korea
[2]Department of Electrical and Electronic Engineering, University of Toyama, Toyama 930-8555, Japan

Corresponding author: Kyoungseok Han (kyoungsh@knu.ac.kr)

This work was supported in part by the National Research Foundation of Korea (NRF) Grant through the Korean Government [Ministry of Science and ICT (MSIT)] under Grant NRF-2021R1A6A1A03043144; and in part by the Brain Korea 21 (BK21) through the Ministry of Education, South Korea, under Grant 4199990314305.

ABSTRACT A good suspension system is of paramount importance to the operating performance of a vehicle and, consequently, to the safety and driving comfort of the passengers. Nevertheless, suspension systems are commonly susceptible to nonlinearity, parameter uncertainty, and exogenous perturbation, which can easily impair their effectiveness. This study first employs a full state feedback super twisting control (FS-STC) to stabilize both vertical displacement and pitch angle of a half-car suspension system in the presence of disturbances. FS-STC inherits the robust property of sliding mode control (SMC) while effectively attenuating the chattering phenomenon as one of its attractive features. However, FS-STC strictly requires both direct displacement and velocity state feedback, which implies additional sensors have to be installed, thus increasing the complexity of the physical structure and being prone to measurement noises. Therefore, a higher order sliding mode observer (HOSMO) based STC (HOSMO-STC) and an unscented Kalman filter (UKF) based STC (UKF-STC) are subsequently proposed to tackle this state availability problem. HOSMO estimates velocity states, thus reducing the dependence on state feedback for STC design. Meanwhile, UKF implementation takes further actions by utilizing more common and easily accessible relative displacements such as suspension strokes to estimate all concerned system states. Comparative simulation results demonstrate that UKF-STC offers better performance in terms of both convergence accuracy and chattering alleviation compared to FS-STC and HOSMO-STC while requiring the least information of state feedback.

INDEX TERMS Half-car suspension, higher-order sliding mode observer, super twisting control, state-feedback critical, unscented Kalman filter.

I. INTRODUCTION

Suspension systems are one of the most important parts of a vehicle, which directly affects vehicle performance in road holding and driving comfort. Locating between the vehicle body and its wheels, a suspension system is responsible for keeping the vehicle balanced in various driving scenarios such as cornering, accelerating, braking, or driving over road bumps or potholes. Therefore, a good suspension system is believed to have a significant impact on passenger safety, vehicle durability, driving maneuver and eventually maintenance cost. Thus, active suspension systems have received considerable attention from researchers throughout the years [1], [2], [3], [4]. While some researchers study on new structures of a suspension system [5], the major concern is on how to design and improve control algorithms for existing physical structures [6], [7], [8], [9].

The primary objective of an active suspension system is to stabilize the attitude of a vehicle in the presence of nonlinearities, parameter uncertainties and external disturbances. Other common objectives include guaranteeing system state constraints so that the criteria of driving comfort and safety can

The associate editor coordinating the review of this manuscript and approving it for publication was Wei Quan.

be satisfied. Various control algorithms have been proposed to achieve these goals, for instance, H_∞ [3], backstepping [1], [4], Fuzzy-PID [10], linear quadratic regulator [11], or sliding mode control (SMC) [6], [12], [13], to name just a few.

As an automotive active suspension system is inherently exposed to several types of disturbances, such as nonlinearity, parameter uncertainty or external perturbation, state estimation and disturbance compensation have always been considered in the literature. In [14], a state differentiator and disturbance estimator are proposed for the sprung mass subsystem of a quarter-car model. Displacement measurements of both sprung and unsprung mass are required in this estimation algorithm, while the continuous control law is derived to actively attenuate the chattering effects. Another disturbance observer that receives both displacement and velocity information of a quarter-car model as inputs is introduced in [15]. The lumped disturbance estimation result is subsequently utilized to enhance the robustness of a terminal SMC, whereas, the chattering phenomenon is passively reduced by improving the observation performance. The task of stabilizing a quarter-car model is tackled slightly different in [16], where the relative displacement (suspension deflection) is the control target, instead of the sprung mass vertical displacement. Consequently, the control scheme requires only the suspension deflection and acceleration as its inputs. An extended super-twisting observer estimating lumped disturbance together with a second-order SMC is then proposed to solve the control problem. Furthermore, the application of a second-order SMC is effective in chattering reduction. Deviating from conventional control methods, [17] employs the ensemble Kalman filter to curb the cost of sensor installation for a quarter-car model. Unmeasured system states are estimated from suspension deflection and acceleration and subsequently used in a super twisting SMC design. It can be interpreted from these papers that the problem of stabilizing an automotive active suspension system can be addressed differently, and that each approach might impose different feedback requirements. Besides, readers who are interested in current advances in state estimation are referred to, for instance, [3], [18], [19], [20] and the references therein.

Backstepping stands out to be one of the most popular control approaches for active suspension systems. An adaptive backstepping control algorithm is introduced in [1] to stabilize both vertical and pitch motions of a half-car suspension model. The proposed algorithm accounts for the hydraulic actuator dynamics and also considers parameter variations in the number of passengers. Another backstepping approach can be found in [4], where integration of an adaptive backstepping technique and a quadratic Lyapunov function is proposed to stabilize the vehicle while actively addressing the safety constraint of road holding. Both above-mentioned papers have an adaptive scheme for parameter adjustment. However, these backstepping algorithms require full-state measurement of the suspension system, which is costly, prone to measurement noise and even unrealistic regarding complexity in installation space and physical structure of the system. Aware of this full-state sensing problem, a higher order sliding mode control proposed in [6] tries to achieve the stabilization objective while using only the relative suspension displacement, such as suspension stroke. The method is believed to be more practical than the full-state-based approach since suspension strokes can be obtained easily. However, [6] raises a concern about the stabilization effectiveness, as the vertical displacement is controlled indirectly via stabilizing the relative displacement between the vehicle body and its unsprung mass. In fact, the method [6] might lack mathematical justification, since the zero relative displacement equation does not have a unique solution. In other words, even if the relative displacement is driven to zero, the vertical displacements of the vehicle body and the unsprung mass can continue to vary at the same value and only die out gradually because of the stabilizing effects of passive springs and shock absorbers. Therefore, although the utilization of relative suspension displacement is more practical than the use of full-state measurement in controller design, the information on the major states such as vertical displacement or pitch angle is still indispensable.

The approach [6] estimates relative velocity and acceleration by a means of a high gain observer. Despite the simplicity, the high gain observer exhibits a drawback of peaking phenomena during the transition period if the initial condition of the real system and that of the observer are different [21]. It is also a common belief that high gains might amplify the undesired noise existing in the measured states, thus degrading the overall control performance, especially in cases of state differentiation. On the other hand, the parameter adaptation schemes found in [1] and [4] are mathematical sounding but model-based, implying that the precision of parameter estimation heavily relies on the accuracy of the model. In other words, the discrepancy between the mathematical modeling and the physical system might deteriorate their precision in parameter estimation and overall stabilization performance in practice. These two cases indicate that a control algorithm designated for nonlinear systems, specifically suspension systems, is required to be robust against uncertainty and measurement noise.

From the above motivation, in this work, we propose and compare three control approaches for the objective of stabilizing a half-car suspension system while considering state availability. Three control algorithms including FS-STC, HOSMO-STC and UKF-STC are selected based on their level of dependence on state-feedback information. FS-STC requires both information of direct measurements of displacement and velocity. HOSMO-STC eases the state feedback requirement by requiring only displacement as it is able to estimate velocities via HOSMO. Meanwhile, UKF-STC represents an indirect output feedback controller as it utilizes only the relative suspension displacement to estimate all system states, reconstructs inner dynamics and disturbance then uses them for controller design. Their control performance including state stabilization precision,

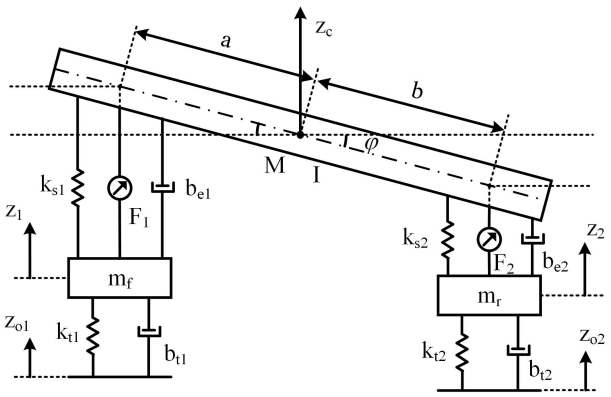

FIGURE 1. Modeling diagram of the considered half-car suspension system [1].

chattering attenuation, road holding and driving comfort are simultaneously evaluated in a comparative simulation.

Modest contributions of the study might include:

- The problem of stabilizing a half-car suspension system in the presence of nonlinearity and disturbance influence is addressed by a super twisting control framework, which is inherently robust and possesses chattering attenuation capability.
- The introduction of HOSMO and UKF in the STC design represents different approaches to reducing the dependence on direct state-feedback information.
- The proposed UKF-STC algorithm satisfactorily controls the suspension system while lifting the burden of state-feedback requirement, which is not readily accessible for the considered suspension system.

The rest of the paper is organized as follows. Section II presents the half-car suspension modeling and control problem statement. Section III introduces three proposed control algorithms including FS-STC, HOSMO-STC and UKF-STC. Section IV provides simulation results and discussion about each controller's advantages and limitations, followed by the conclusion and future work in Section V.

II. SYSTEM MODELING AND PROBLEM STATEMENT

A. SYSTEM DESCRIPTION

The half-car suspension system considered in this study is illustrated in Fig. 1. In this figure, several parameters used to model the suspension are as follows. M denotes the sprung mass of the vehicle body, and I is the mass moment of inertia associated with the pitch motion. m_f and m_r stand for the front and rear unsprung masses, respectively. The stiffness and damping coefficients of the suspension are k_{si} and b_{ei}, $(i = 1, 2)$, respectively. Similarly, k_{ti} and b_{ti}, $(i = 1, 2)$ represent the compressibility and damping coefficients of the tires, respectively. Motions of the vehicle body are indicated by z_c for the vertical displacement and φ for its pitch angle. While z_1 and z_2 are the displacements of the unsprung mass, z_{o1} and z_{o2} are the road inputs to the wheels of the given model, accordingly. Active control actions impact the system via two forces F_1 and F_2 locating respectively at a distance a and b from the center of mass of the vehicle. Further details of the model can be found in [1] and the references therein.

The suspension system is modeled using the first principles as follows.

1) Unsprung mass subsystems m_f, m_r: these subsystems are modeled as spring-mass-damper systems, whose dynamic equations are given as

$$\begin{aligned} m_f\ddot{z}_1 &= k_{s1}\Delta y_1 + b_{e1}\Delta\dot{y}_1 \\ &\quad - k_{t1}(z_1 - z_{o1}) - b_{t1}(\dot{z}_1 - \dot{z}_{o1}) - F_1 \qquad (1) \\ m_r\ddot{z}_2 &= k_{s2}\Delta y_2 + b_{e2}\Delta\dot{y}_2 \\ &\quad - k_{t2}(z_2 - z_{o2}) - b_{t2}(\dot{z}_2 - \dot{z}_{o2}) - F_2 \qquad (2) \end{aligned}$$

where Δy_i and $\Delta\dot{y}_i$, $(i = 1, 2)$ denote the relative suspension displacements and velocities of the following forms:

$$\Delta y_1 = z_c + a\sin\varphi - z_1, \;\; \Delta\dot{y}_1 = \dot{z}_c + a\dot{\varphi}\cos\varphi - \dot{z}_1 \quad (3)$$
$$\Delta y_2 = z_c - b\sin\varphi - z_2, \;\; \Delta\dot{y}_2 = \dot{z}_c - b\dot{\varphi}\cos\varphi - \dot{z}_2 \quad (4)$$

2) Sprung mass subsystems M: these subsystems include springs, shock absorbers and actuators that absorb and generate forces between the vehicle body and the road. The dynamics of the sprung mass subsystem can be expressed as

$$\begin{cases} M\ddot{z}_c = -\phi_1(t) + F_1 + F_2 \\ I\ddot{\varphi} = -\phi_2(t) + aF_1 - bF_2 \end{cases} \qquad (5)$$

with

$$\begin{aligned} \phi_1(t) &= k_{s1}\Delta y_1 + k_{s2}\Delta y_2 + b_{e1}\Delta\dot{y}_1 + b_{e2}\Delta\dot{y}_2 \\ \phi_2(t) &= a(k_{s1}\Delta y_1 + b_{e1}\Delta\dot{y}_1) - b(k_{s2}\Delta y_2 + b_{e2}\Delta\dot{y}_2) \end{aligned}$$

B. PROBLEM STATEMENT

The primary objective of the suspension control system is to stabilize the vehicle. Specifically, the control design aims to drive both the vertical displacement, z_c, and the pitch angle, φ, to equilibrium and keep them thereafter.

$$\lim_{t\to\infty} z_c = 0 \quad \text{or} \quad \text{bounded}.$$
$$\lim_{t\to\infty} \varphi = 0 \quad \text{or} \quad \text{bounded}.$$

Other objectives include driving comfort, where vertical and pitch accelerations are kept to relatively small values, and road holding, where the dynamic loads exerted on the tires are regulated not to exceed their static loads. These objectives can be expressed as follows.

$$\left|\frac{k_{ti}(z_i - z_{oi}) + b_{ti}(\dot{z}_i - \dot{z}_{oi})}{S_i}\right| < 1, \quad i = 1, 2 \qquad (6)$$

where S_i, $i = 1, 2$ are static loads with following formula:

$$S_1 = \frac{Mgb}{(a+b)} + m_f g \qquad (7)$$
$$S_1 + S_2 = (M + m_f + m_r)g. \qquad (8)$$

III. CONTROL ALGORITHM DESIGN

A. CONTROL-ORIENTED MODELING

The suspension system dynamics expressed at (1), (2) and (5) can be rearranged into a general second-order canonical form as

$$\begin{cases} \dot{X}_1 = X_2 \\ \dot{X}_2 = H\left(X_1, X_2\right) + GU + D \end{cases} \tag{9}$$

where $X_1 = [z_c,\ \varphi]^{\mathrm{T}}$ and $X_2 = [\dot{z}_c,\ \dot{\varphi}]^{\mathrm{T}}$ are the controlled system states, $H\left(X_1, X_2\right)$ denotes the internal dynamics matrix, G is the control matrix, and D represents the lumped disturbance of the following form:

$$\begin{aligned} H &= A_X X_1 + B_X X_2 \\ A_X &= \begin{bmatrix} -(k_{s1}+k_{s2})/M & -(ak_{s1}-bk_{s2})/M \\ -(ak_{s1}-bk_{s2})/I & -\left(a^2k_{s1}+b^2k_{s2}\right)/I \end{bmatrix} \\ B_X &= \begin{bmatrix} -(b_{e1}+b_{e2})/M & -(ab_{e1}-bb_{e2})/M \\ -(ab_{e1}-bb_{e2})/I & -\left(a^2b_{e1}+b^2b_{e2}\right)/I \end{bmatrix} \\ G &= \begin{bmatrix} 1/M & 1/M \\ a/I & -b/I \end{bmatrix} \\ D &= \begin{bmatrix} k_{s1}/M & k_{s2}/M \\ ak_{s1}/I & -bk_{s2}/I \end{bmatrix} \begin{bmatrix} z_1 \\ z_2 \end{bmatrix} \\ &\quad + \begin{bmatrix} b_{e1}/M & b_{e2}/M \\ ab_{e1}/I & -bb_{e2}/I \end{bmatrix} \begin{bmatrix} \dot{z}_1 \\ \dot{z}_2 \end{bmatrix} \\ &\quad + \begin{bmatrix} ak_{s1}-bk_{s2} & ab_{e1}-bb_{e2} \\ a^2k_{s1}+b^2k_{s2} & a^2b_{e1}+b^2b_{e2} \end{bmatrix} \begin{bmatrix} \sin\varphi - \varphi \\ \dot{\varphi}\left(\cos\varphi - \varphi\right) \end{bmatrix} \end{aligned} \tag{10}$$

It can be interpreted from above matrices that the lumped disturbance D contains unmodeled terms z_i, $\dot{z}_i$, $(i = 1, 2)$, which we cannot account into the internal dynamics because of the lack of measurement.

B. CONTROL CANDIDATES

Concerning the availability of displacement/velocity sensing in practice, in this study, the following three controllers are considered successively.

- Full state feedback super twisting control (FS-STC): both displacement, $[z_c,\ \varphi]^{\mathrm{T}}$, and velocity, $[\dot{z}_c,\ \dot{\varphi}]^{\mathrm{T}}$, measurements are available.
- (Semi-state feedback) Higher order sliding mode observer-based super-twisting control (HOSMO-STC): only displacement, $[z_c,\ \varphi]^{\mathrm{T}}$, is available, and velocity, $[\dot{z}_c,\ \dot{\varphi}]^{\mathrm{T}}$, is estimated using HOSMO.
- (Indirect state feedback) Unscented Kalman filter-based super-twisting control (UKF-STC): both displacement, $[z_c,\ \varphi]^{\mathrm{T}}$, and velocity, $[\dot{z}_c,\ \dot{\varphi}]^{\mathrm{T}}$, are not available but estimated from relative displacements (suspension strokes), $\Delta y_1 = z_c + a\sin\varphi - z_1$ and $\Delta y_2 = z_c - b\sin\varphi - z_2$, using UKF.

The overall diagram of the proposed control approach is illustrated in Fig. 2, where three proposed controllers are attached with different feedback input requirements.

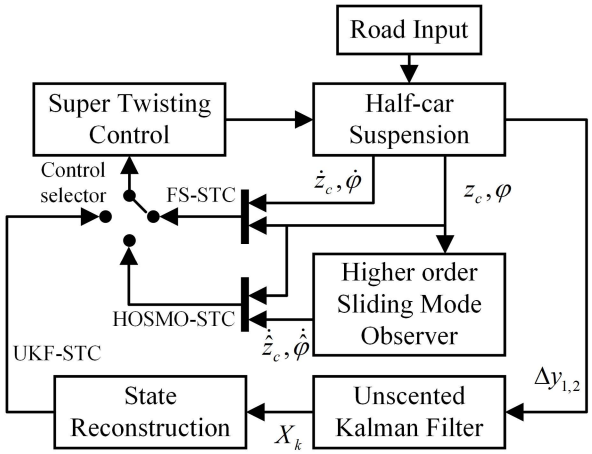

FIGURE 2. Comparative control diagram of three considered algorithms with different state feedback indication.

1) FS-STC FORMULATION

The following linear sliding surface with full information on the displacement and velocity states is considered for the FS-STC.

$$S = C_1 X_1 + X_2 \tag{11}$$

Taking the derivative of the sliding surface (11) and substituting the system dynamics (9) into the derived equation, we obtain:

$$\begin{aligned} \dot{S} &= C_1\dot{X}_1 + \dot{X}_2 \\ &= C_1 X_2 + (H + GU + D). \end{aligned} \tag{12}$$

Consequently, the following X_1 and S coordinate can be established.

$$\begin{aligned} \dot{X}_1 &= S - C_1 X_1 \\ \dot{S} &= C_1 X_2 + (H + GU + D). \end{aligned} \tag{13}$$

Accordingly, to realize the second-order sliding mode or super-twisting control, a control law can be designed as

$$\begin{aligned} U = G^{-1}(&-C_1 X_2 - H \\ &- \lambda_1 |S|^{1/2} sign(S) - \int_0^t \lambda_2 sign(S) d\tau) \end{aligned} \tag{14}$$

where λ_1 and λ_2 are tuning control gains. Substituting the control law (14) into (13), the closed-loop dynamics in X and S coordinate now becomes:

$$\begin{aligned} \dot{X}_1 &= S - C_1 X_1 \\ \dot{S} &= -\lambda_1 |S|^{1/2} sign\,(S) + Z \\ \dot{Z} &= \lambda_2 sign\,(S) + \dot{D}. \end{aligned} \tag{15}$$

If the control gains are properly selected such that $\lambda_1 = 1.5\sqrt{\Delta_1}$ and $\lambda_2 = 1.1\Delta_1$ with $\max|\dot{D}| < \Delta_1$, then the last two equations of (15) forms a super twisting algorithm (STA) [22], [23]. Consequently, the sliding mode, $S = \dot{S} = 0$ will occur, implying that

$$\begin{aligned} \dot{X}_1 &= -C_1 X_1 \\ X_2 &= -C_1 X_1. \end{aligned}$$

Thus, the system states X_1 and X_2 will asymptotically converge to zero.

2) HOSMO-STC FORMULATION

The FS-STC design is straight-forward but requires displacement and velocity state feedback information of both vertical and pitch velocities, which can be obtained by velocity sensors or numerical differentiation. However, additional sensors are costly and add complexity to the physical system, and numerical differentiation amplifies measurement noise. Thus, it is more beneficial to implement an observer to estimate the velocities.

An HOSMO formulation [24] is constructed based on the system dynamics (9) as follows:

$$\begin{cases} \dot{\hat{X}}_1 = \hat{X}_2 + Z_1 \\ \dot{\hat{X}}_2 = \hat{X}_3 + \hat{H} + GU + Z_2 \\ \dot{\hat{X}}_3 = Z_3 \end{cases} \tag{16}$$

where $\hat{X}_{1,2}$ are the estimate of system states $X_{1,2}$, and $\hat{X}_3$ estimates the lumped disturbance; $Z_i (i = 1, 2, 3)$ are the correction terms of the forms:

$$\begin{aligned} Z_1 &= \begin{bmatrix} k_{11}|E_1(1)|^{2/3} sign(E_1(1)) \\ k_{12}|E_1(2)|^{2/3} sign(E_1(2)) \end{bmatrix} \\ &= K_1|E_1|^{2/3} sign(E_1) \qquad (17) \\ Z_2 &= K_2|E_1|^{1/3} sign(E_1) \qquad (18) \\ Z_3 &= K_3 sign(E_1) \qquad (19) \end{aligned}$$

with $E_1 = X_1 - \hat{X}_1$ being the first estimation error. Other estimation errors include $E_2 = X_2 - \hat{X}_2$, and $E_3 = (H - \hat{H}) + D - \hat{X}_3$. For simplicity, observer gains $K_i (i = 1, 2, 3)$ are selected to be scalars. Consequently, with velocity state estimated from HOSMO, a sliding surface is designed as

$$\hat{S} = C_1 X_1 + \hat{X}_2 \tag{20}$$

Differentiating the sliding surface (20) and subsequently applying the system dynamics (9) and the observer dynamics (16), we obtain:

$$\begin{aligned} \dot{\hat{S}} &= C_1 \dot{X}_1 + \dot{\hat{X}}_2 \\ &= C_1 X_2 + (\hat{X}_3 + \hat{H} + GU + Z_2). \end{aligned} \tag{21}$$

Accordingly, a control law can be designed in the following form.

$$\begin{aligned} U = G^{-1}(&-C_1 \hat{X}_2 - \hat{X}_3 - \hat{H} + Z_2 \\ &- \lambda_1 \left|\hat{S}\right|^{1/2} sign(\hat{S}) + \int_0^t \lambda_2 sign(\hat{S}) d\tau) \end{aligned} \tag{22}$$

Taking into account (22), the presence of $\hat{X}_3$ in the control law indicates that HOSMO-STC actively compensates for the lumped disturbance. Subsequently, applying the above control law into the system, we obtain the following closed-loop dynamics:

$$\begin{aligned} \Xi : &\begin{cases} \dot{E}_1 = -K_1|E_1|^{2/3} sign(E_1) + E_2 \\ \dot{E}_2 = -K_2|E_1|^{1/3} sign(E_1) + E_3 \\ \dot{E}_3 = -K_3 sign(E_1) + \dot{D} + (\dot{H} - \dot{\hat{H}}) \end{cases} \\ \Pi : &\begin{cases} \dot{X}_1 = \hat{S} - C_1 X_1 + E_2 \\ \dot{\hat{S}} = C_1 E_2 - \lambda_1 \left|\hat{S}\right|^{1/2} sign(\hat{S}) + Z \\ \dot{Z} = -\lambda_2 sign(\hat{S}) \end{cases} \end{aligned} \tag{23}$$

where Ξ and Π represent the observer error dynamics and X_1-$\hat{S}$ coordinate dynamics, respectively. Investigating Π, it has been proved in [24] that the STA will not occur unless the estimation error E_2 is driven to zero first. Therefore, observer gains $K_i (i = 1, 2, 3)$ must be appropriately selected for the finite-time convergence of the observer. For instance, they can be selected as $K_1 = \rho_1 L^{1/3}$, $K_2 = \rho_2 L^{1/2}$, and $K_3 = \rho_3 L$, where $\rho_i (i = 1, 2, 3)$ are properly chosen for the observer convergence, and L is the Lipschitz constant of the lumped disturbance/state, which is can be tuned for satisfactory control performance [25]. Once the finite-time convergence of the HOSMO happens, $E_2 = 0$. Substituting this into Π yields:

$$\Pi : \begin{cases} \dot{X}_1 = \hat{S} - C_1 X_1 \\ \dot{\hat{S}} = -\lambda_1 \left|\hat{S}\right|^{1/2} sign(\hat{S}) + Z \\ \dot{Z} = -\lambda_2 sign(\hat{S}) \end{cases} \tag{24}$$

Provided that $\lambda_i > 0$, $i = 1, 2$ are selected properly, the last two equations of (24) form an STA, and $\hat{S} = \dot{\hat{S}} = 0$ is guaranteed to occur in finite time. Consequently, system states will asymptotically converge to zeros, as shown in the previous subsection. It is worth noting that unlike FS-STC, HOSMO-STC does not require control gains $\lambda_i > 0$, $i = 1, 2$ to be considerably large to compensate for the disturbance's influence. However, for the convergence of HOSMO, the observer gains $K_i (i = 1, 2, 3)$ must be large instead, which still implies a risk of chattering phenomena in the control signal. This happens as a result of the presence of the term $Z_2 = K_2|E_1|^{1/3} sign(E_1)$ in the control law (22). This remark will be vividly illustrated in the simulation results.

3) UKF-STC DESIGN

The application of HOSMO has partially lifted the burden of state feedback requirement for the STC design. However, HOSMO-STC still requires measurements of the vertical displacement and pitch angle of the vehicle body. This section introduces a more practical control approach, as UKF is employed to estimate all states of the system. The proposed method uses only relative displacements that can be easily obtained from measuring suspension strokes and utilizes the following equations in its formulation.

UKF-oriented system state:

$$X_k = \begin{bmatrix} z_c & \dot{z}_c & \varphi & \dot{\varphi} & z_1 & \dot{z}_1 & z_2 & \dot{z}_2 \end{bmatrix}^{\mathrm{T}} \tag{25}$$

State transition function (discretized by the Euler method):

$$X_k = F(X_{k-1}) + W \tag{26}$$

where W is assumed to be an additive process noise, $W(0, Q)$, and $F_X(X_{k-1})$ is of the following formulation:

$$F(X_{k-1}) = X_{k-1} + \begin{bmatrix} X_{k-1}(2) \\ (1/M)(-\phi_1 + F_1 + F_2) \\ X_{k-1}(4) \\ (1/I)(-\phi_1 + F_1 + F_2) \\ X_{k-1}(6) \\ (1/m_f)(k_{s1}\Delta y_1 + b_{e1}\Delta\dot{y}_1 - F_1) \\ X_{k-1}(8) \\ (1/m_r)(k_{s2}\Delta y_2 + b_{e2}\Delta\dot{y}_2 - F_2) \end{bmatrix} T_s$$

with T_s is the sampling time constant.

Measurement function:

$$\begin{aligned} Y_k &= \begin{bmatrix} \Delta y_1 \\ \Delta y_2 \end{bmatrix} + V \\ &= \begin{bmatrix} X_k(1) + a\sin X_k(3) - X_k(5) \\ X_k(1) - b\sin X_k(3) - X_k(7) \end{bmatrix} + V \\ &= J(X_k) + V \end{aligned} \tag{27}$$

where $V(0, R)$ is the additive measurement noise. Using the above equations, a standard UKF algorithm estimates system states with the following procedure [26].

Initialization:

$$\begin{aligned} \hat{X}_0 &= \mathrm{E}[X_0] \\ P_0 &= \mathrm{E}\left[(X_0 - \hat{X}_0)(X_0 - \hat{X}_0)^{\mathrm{T}}\right] \end{aligned}$$

Sigma point calculation:

$$\chi_{k-1} = \left[\hat{X}_{k-1}\ \hat{X}_{k-1} + \eta\sqrt{P_{k-1}}\ \hat{X}_{k-1} - \eta\sqrt{P_{k-1}}\right]$$

Time update:

$$\begin{aligned} \chi_{k|k-1} &= F(\chi_{k-1}) \\ \hat{X}_k^- &= \sum_{i=0}^{2N} \omega_i^{(m)} \chi_{i,k|k-1} \\ P_k^- &= \sum_{i=0}^{2N} \omega_i^{(c)} [\chi_{i,k|k-1} - \hat{X}_k^-][\chi_{i,k|k-1} - \hat{X}_k^-]^T + Q \\ \Upsilon_{k|k-1} &= J(\chi_{k|k-1}) \\ \hat{Y}_k^- &= \sum_{i=0}^{2N} \omega_i^{(m)} \Upsilon_{i,k|k-1} \end{aligned}$$

Measurement update:

$$\begin{aligned} P_{\tilde{Y}_k\tilde{Y}_k} &= \sum_{i=0}^{2N} \omega_i^{(c)} [\Upsilon_{i,k|k-1} - \hat{Y}_k^-][\Upsilon_{i,k|k-1} - \hat{Y}_k^-]^{\mathrm{T}} + R \\ P_{X_kY_k} &= \sum_{i=0}^{2N} \omega_i^{(c)} [\chi_{i,k|k-1} - \hat{X}_k^-][\Upsilon_{i,k|k-1} - \hat{Y}_k^-]^{\mathrm{T}} \\ \mathrm{K}_k &= P_{X_kY_k} P_{\tilde{Y}_k\tilde{Y}_k}^{-1} \\ \hat{X}_k &= \hat{X}_k^- + \mathrm{K}_k(Y_k - \hat{Y}_k^-) \\ P_k &= P_k^- - \mathrm{K}_k P_{\tilde{Y}_k\tilde{Y}_k} \mathrm{K}_k^{\mathrm{T}} \end{aligned}$$

where $N = 8$ is the state dimension, $\lambda = N(\alpha^2 - 1)$ and $\eta = \sqrt{N + \lambda}$ are scaling factors, and ω_i is a scalar weight set satisfying:

$$\begin{aligned} \omega_0^{(m)} &= \lambda/(N + \lambda) \\ \omega_0^{(c)} &= \lambda/(N + \lambda) + (1 - \alpha^2 + \beta) \\ \omega_i^{(m)} &= 7\omega_i^{(c)} = 1/[2(N + \lambda)] \end{aligned}$$

where m and c stand for mean and covariance, respectively, $i = 1, 2, \ldots, 2N$.

With estimation results obtained from the UKF, the system states $X_i\,(i = 1, 2)$ (9) and the lumped disturbance D (10) can be now estimated. Subsequently, a sliding surface can be designed accordingly as follows.

$$\hat{S} = C_1\hat{X}_1 + \hat{X}_2 \tag{28}$$

where $\hat{X}_i\,(i = 1, 2)$ are the states of the system reconstructed from UKF.

Taking the derivative of the sliding surface (28) yields:

$$\begin{aligned} \dot{\hat{S}} &= C_1\dot{\hat{X}}_1 + \dot{\hat{X}}_2 \\ &= C_1(\dot{X}_1 - \dot{\tilde{X}}_1) + (\dot{X}_2 - \dot{\tilde{X}}_2) \\ &= C_1X_2 - C_1\dot{\tilde{X}}_1 + (H + GU + D) - \dot{\tilde{X}}_2 \end{aligned} \tag{29}$$

where $\tilde{X}_i = X_i - \hat{X}_i,\ (i = 1, 2)$ denote UKF state estimation errors.

From the above sliding surface derivative equation, a control law can be designed accordingly as follows.

$$\begin{aligned} U = G^{-1}(&-C_1\hat{X}_2 - \hat{H} - \hat{D} \\ &- \lambda_1|S|^{1/2}sign(S) - \int_0^t \lambda_2 sign(S)\,d\tau) \end{aligned} \tag{30}$$

Substituting the control law (30) into (29) results in the following closed-loop dynamics:

$$\begin{cases} \dot{\hat{S}} = -\lambda_1|S|^{1/2}sign(\hat{S}) + Z \\ \dot{Z} = -\lambda_2 sign(\hat{S}) + (C_1\dot{\hat{X}}_2 - C_1\ddot{\tilde{X}}_1 + \dot{\hat{H}} - \ddot{\tilde{X}}_2 + \dot{\tilde{D}}) \end{cases} \tag{31}$$

If the control parameters λ_1 and λ_2 are properly selected such that the effects of estimation errors $\tilde{X}_1$, $\tilde{X}_2$, $\tilde{H}$, $\tilde{D}$ are compensated, e.g. $\lambda_1 = 1.5\sqrt{\Delta_2}$ and $\lambda_2 = 1.1\Delta_2$ with $\max|C_1\ddot{\tilde{X}}_1 + \dot{\tilde{H}} - \ddot{\tilde{X}}_2 + \dot{\tilde{D}}| \le \Delta_2$, then the second order sliding mode will happen [22], [23]. Once $\hat{S} = \dot{\hat{S}} = 0$, it follows that:

$$\begin{aligned} C_1\hat{X}_1 + \hat{X}_2 &= 0 \\ C_1X_1 + \dot{X}_1 &= C_1\tilde{X}_1 + \tilde{X}_2 \end{aligned} \tag{32}$$

Assume here that the UKF estimation errors are bounded, satisfying $\max|C_1\tilde{X}_1 + \tilde{X}_2| \le \Delta_3$. Then, it can derive from the above equation that

$$\begin{aligned} X_1(t) &\le \frac{\Delta_3}{C_1} - \frac{X_1(0)}{C_1}e^{-C_1t} \\ \lim_{t\to\infty} X_1(t) &\le \lim_{t\to\infty}\left(\frac{\Delta_3}{C_1} - \frac{X_1(0)}{C_1}e^{-C_1t}\right) \le \frac{\Delta_3}{C_1} \end{aligned}$$

TABLE 1. Nominal parameters used for modeling the half-car suspension system [1].

Parameter	Value	Parameter	Value
M	1200 kg	I	600 kgm^2
m_f	100 kg	m_r	100 kg
k_{s1}	15000 N/m	k_{s2}	15000 N/m
b_{e1}	2500 Ns/m	b_{e2}	2500 Ns/m
k_{t1}	2×10^5 N/m	k_{t2}	2×10^5 N/m
b_{t1}	1000 Ns/m	b_{t2}	1000 Ns/m
a	1.2 m	b	1.5 m

where $X_1(0) = X_1(t = 0)$ is the initial condition of the system state.

The above inequality indicates that the system states can be driven to an arbitrarily small region around the equilibrium, provided that the UKF parameters are well tuned and a sufficiently large control gain C_1 is selected. Moreover, the benefit of a sufficiently large control gain C_1 is twofold. It not only shortens the state convergence time, but also minimizes the steady-state stabilizing errors of the system.

IV. SIMULATION RESULTS AND DISCUSSION

A. ROAD PROFILE AND PARAMETER SELECTION

To evaluate the performance of the proposed control algorithms, the half-car suspension system and three control candidates are constructed in the MATLAB-Simulink environment. Table 1 summarizes the values of all parameters used for system modeling.

The classical bumped road profiles chosen to verify the effectiveness of the proposed controllers are borrowed from [1] and of the following form.

$$z_{oi} = \begin{cases} \frac{h_b[1-cos(6\pi t)]}{2}, & t \in T_i \\ 0, & otherwise \end{cases} \tag{33}$$

where $z_{oi}(i = 1, 2)$ represent the ground displacement inputs to the front and rear wheel, respectively. $h_b = 2\,cm$ denotes the magnitude of the bump road. $T_i\,(i = 1, 2)$ represents the time periods for the front and rear wheels, that is, $T_1 = [1\,s,\ 1.25\,s]$ and $T_2 = [1 + \Delta_t\,s,\ 1.25 + \Delta_t\,s]$. $\Delta_t = (a + b)/V_0$ stands for the time constant between the front and rear wheel, with $V_0 = 20$ m/s is the constant speed of the vehicle.

Table 2 records the control gains dedicated to each control candidate. In addition to that, a process noise covariance $Q = 10^{-8} \times diag([0.1, 1, 0.1, 1, 1, 5 \times 10^6, 5 \times 10^6])$ and a measurement noise covariance of $R = 10^{-6} \times diag([1, 1])$ are selected by the trial and error method for the UKF.
The principal sampling time is chosen to be 10^{-4} s, and the ODE4 Runge-Kutta is set to be the solver.

B. COMPARATIVE SIMULATION RESULTS

Fig. 3 demonstrates vertical displacement and pitch angle stabilization precision of the three controllers. It is easy to point

TABLE 2. Selection of control parameters for three controller candidates.

Parameters	FS-STC	HOSMO-STC	UKF-STC
C_1	15	15	15
λ_1	$1.5 \times \sqrt{300}$	2	$1.5 \times \sqrt{20}$
λ_2	1.1×300	2	1.1×20
K_1		$4 \times 65^{1/3}$	
K_2		$11 \times 65^{1/2}$	
K_3		4×65	

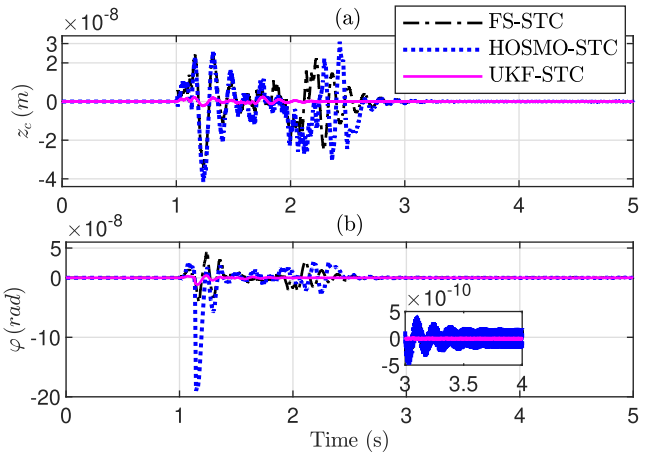

FIGURE 3. Control performance of three considered control candidates in stabilizing (a) vertical displacement. (b) pitch motion.

out that UKF-STC outperforms FS-STC and HOSMO-STC in terms of both convergence time and accuracy. Under the impact of road bump disturbance at 1 s, the vertical and pitch motions of UKF-STC oscillate in a bound of 2.5×10^{-9} m and 4.0×10^{-9} rad, respectively. Meanwhile, the figures for FS-STC and HOSMO-STC are approximately ten times or higher their UKF-STC. UKF-STC trajectory also exhibits much less chattering than the other two counterparts, which can be interpreted from the subplot.

Fig. 4 illustrates the vertical and pitch acceleration time record, which is believed to directly affect driving comfort. It can be seen from Fig. 4 that UKF-STC exhibits superior performance in acceleration minimization compared to the other two control algorithms. Fig. 4 also shows the undesired chattering phenomena in the trajectories of FS-STC and HOSMO-STC even after contact time with the bumped part of the road. This indicates that a sacrifice of smoothness has been made for the sake of robustness in FS-STC and HOSMO-STC design. Meanwhile, UKF-STC does not suffer from this phenomenon and shows almost consistency in its trajectories.

Safety concerns can be assessed in Fig. 5, where the ratios of dynamic and static loads of all controller candidates are compared. It can be interpreted from Fig. 5 that all controllers satisfy the safety constraint, since the load ratios are all less than 1, satisfying the requirement (6).

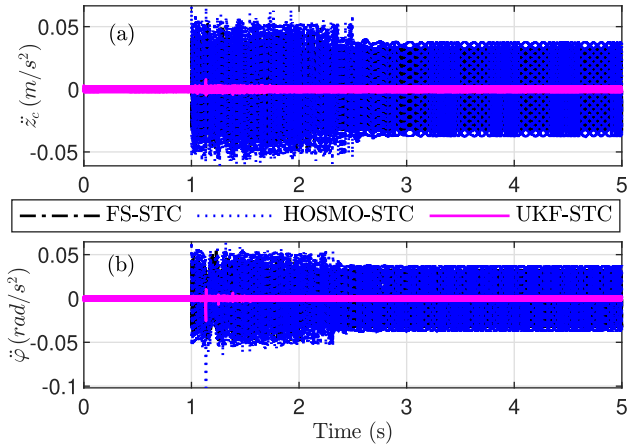

FIGURE 4. Riding comfort criterion in terms of acceleration minimization of all controllers. (a) Vertical acceleration. (b) Pitch acceleration.

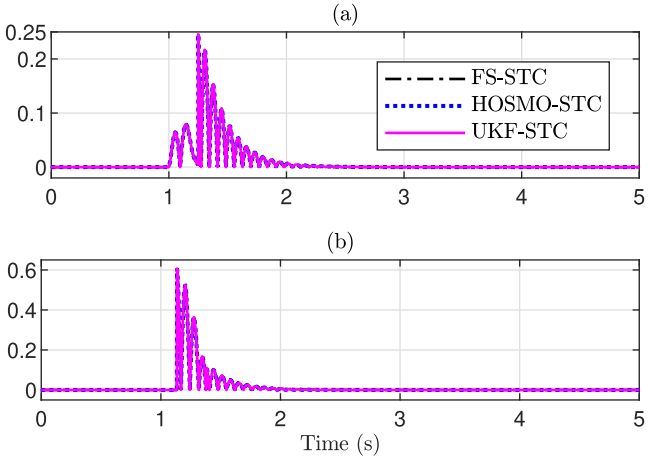

FIGURE 5. Road-holding requirement with dynamic and static load ratio of all controllers. (a) Front wheel. (b) Rear wheel.

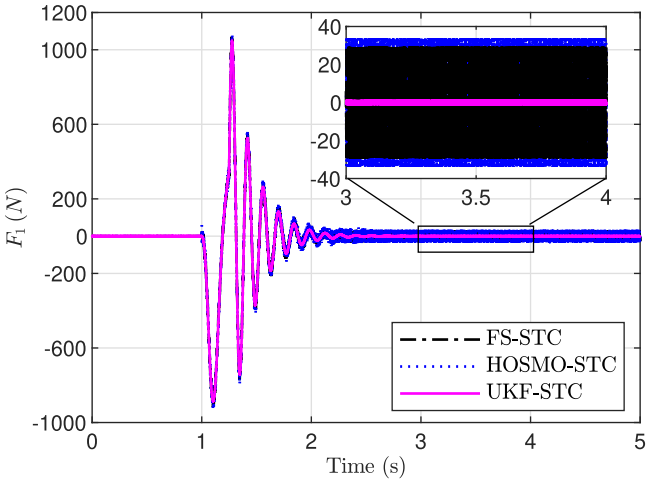

FIGURE 6. Front-wheel control input comparison in the form of ideal force generation.

Control signal trajectories, which represent the ideal force generation of all control algorithms, are depicted in Fig. 6 and Fig. 7. Although their overall shapes are similar, there

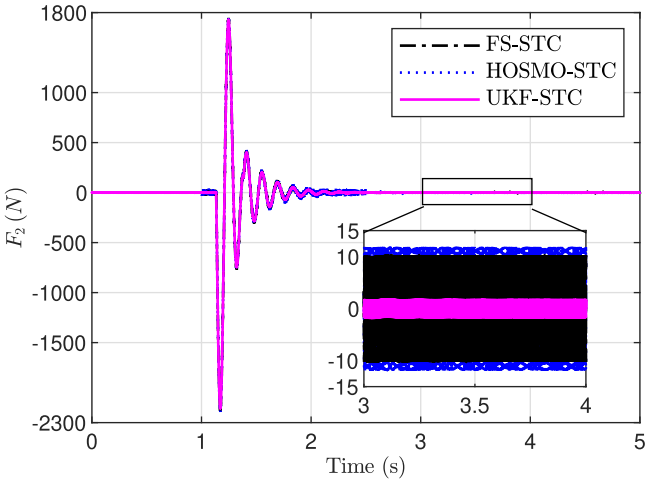

FIGURE 7. Rear-wheel control input comparison in the form of ideal force generation.

TABLE 3. Root-mean-square (RMS) errors in state estimation of UKF and HOSMO.

State	UKF	HOSMO
z_c	1.0823×10^{-11}	7.9749×10^{-11}
$\dot{z}_c$	1.4967×10^{-8}	2.2114×10^{-6}
φ	2.8875×10^{-11}	10.593×10^{-11}
$\dot{\varphi}$	3.8779×10^{-8}	2.3431×10^{-6}
z_1	3.2234×10^{-9}	
$\dot{z}_1$	2.7451×10^{-4}	
z_2	5.9705×10^{-9}	
$\dot{z}_2$	5.1278×10^{-4}	

is a striking difference in their magnitude. Specifically, both FS-STC and HOSMO-STC exhibit considerably larger chattering effect in their control signals compared to UKF-STC. The chattering in their trajectories might pose a serious challenge when the actuator dynamics is considered and designed to track these ideal forces.

The state estimation accuracy of HOSMO and UKF are shown in Fig. 8 and Fig. 9, respectively. The chattering phenomenon in the trajectory can be seen for the case of HOSMO but not for the case of UKF indicates that UKF has better state estimation performance. Table 3 compares their Root-Mean-Square (RMS) errors in state estimation, where UKF outperforms HOSMO in terms of both precision and the number of state estimated.

The influence of different gain selections on control performance of UKF-STC algorithm is illustrated in Fig. 10 and Table 4. It is clear that the simulation results agree with the statement made earlier in the UKF-STC stability analysis that increasing C_1 helps to minimize convergence time and tracking error.

Ultimately, Fig. 11 captures the robustness of three candidate controllers in noisy measurement and uncertain system

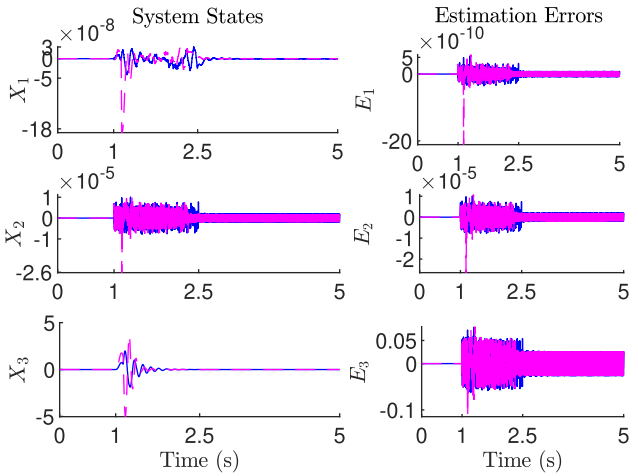

FIGURE 8. State estimation performance of HOSMO with vector state trajectories on the left side and their estimation errors on the right side of the figure.

parameters. In this case, a Gaussian measurement noise with mean of 0 and variance of 9×10^{-12}, a change in vehicle mass $M = 1000\,\text{kg}$ and mass moment of inertia $I = 500\,\text{kgm}^2$ are included in the system model. Except that, all simulation conditions and control gains are kept to be the same as the previous study. The result in Fig. 11 shows that, compared to Fig. 3, control performance degrades significantly for all controllers. FS-STC appears to produce the smallest stabilizing errors. However, it is worth noting that the accuracy of FS-STC comes with the price of full-state feedback information and with high control gains requirements, as shown in Table 2. Meanwhile, UKF-STC performance is still comparable to that of HOSMO-STC and FS-STC. In addition, the UKF-STC trajectory is more stable and chattering-reduced compared to the other two.

C. DISCUSSION

One might find it tempting to directly stabilize the relative displacements Δy_1 (3), Δy_2 (4), hoping that the vehicle body would be stabilized in terms of both vertical and pitch motion, as reported in [6]. This is because the use of only relative displacements for an output-feedback controller makes this approach seem appealing. However, the approach appears to be invalid. The formulation of Δy_1 (3) and Δy_2 (4) indicate that the convergence of both vertical and pitch motions leads to the stabilization of the front and rear wheel relative displacements. Unfortunately, the reverse direction is not correct. The method lacks mathematical justification as

$$\Delta y_1 = z_c + a\sin\varphi - z_1 = 0$$
$$\Delta y_2 = z_c - b\sin\varphi - z_2 = 0$$

is a set of two equations with four variables, thus implying no unique solutions can be obtained. In fact, if Δy_1 and Δy_2 are directly stabilized, z_c, φ and z_i, $i = 1, 2$ could continue to vary without convergence to zero in such a way that they still satisfy the equation set. For example, a set

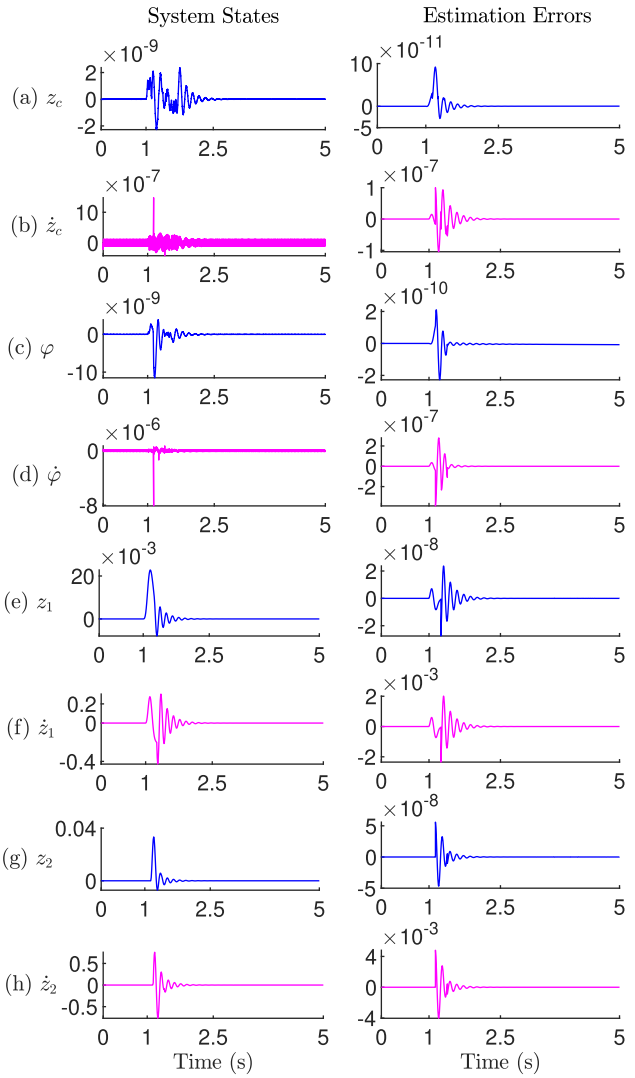

FIGURE 9. State estimation performance of UKF with individual states on the left side and their estimation errors on the right side. (a) Vertical displacement, (b) Vertical velocity, (c) Pitch motion, (d) Pitch velocity, (e) Front unsprung mass displacement, (f) Front unsprung mass velocity, (g) Rear unsprung mass displacement, (h) Rear unsprung mass velocity.

of solutions could be $\varphi = 0$ and $z_c = z_1 = z_2 = \xi_z$, where ξ_z is an arbitrary constant. This observation is further demonstrated in Fig. 12, where the relative displacements affected by the road bump (33) are almost immediately stabilized by the FS-STC algorithm. However, since the vertical and pitch motions are not directly targeted, they continue to oscillate and only gradually die out because of the passive damper-spring elements. Therefore, it is concluded here that the information of the vertical displacement z_c and pitch angle φ are necessary in order to stabilize the vehicle, thus justifying the use of the UKF-STC scheme proposed in this paper.

Another aspect worth considering is the cause of success of the proposed approach. The comparative simulation results have demonstrated the superiority of UKF-STC over FS-STC and HOSMO-STC in suspension stabilization. This statement can be explained as follows. Although FS-STC

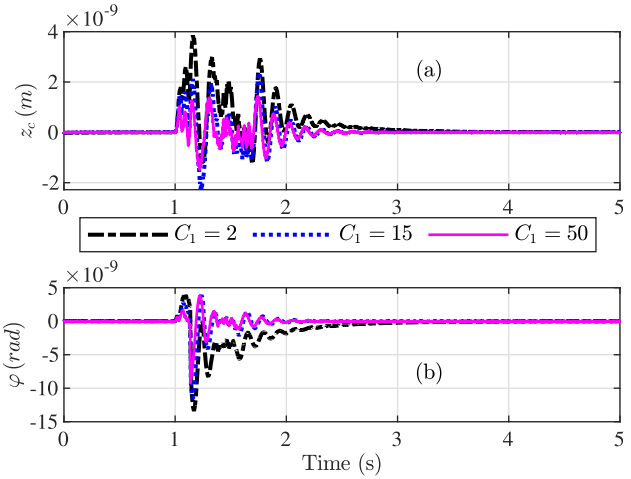

FIGURE 10. Stabilizing performance improvement with increasing control parameter C_1 in UKF-STC formulation. (a) Vertical displacement. (b) Pitch Motion.

TABLE 4. Corresponding RMS value of system states with different selection of control gain C_1 in UKF-STC formulation.

RMS ($\times 10^{-10}$)	$C_1 = 2$	$C_1 = 15$	$C_1 = 50$
z_c	7.1675	4.6574	2.8701
φ	20.1031	12.0225	7.7269

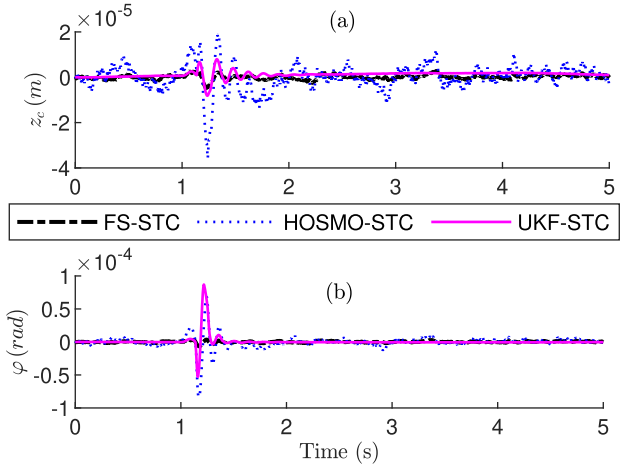

FIGURE 11. Stabilization performance deteriorated by noisy measurement and parameter uncertainty. (a) Vertical displacement. (b) Pitch motion.

has both displacement and velocity measurements, the ignorance of lumped disturbance in control design (14) force its control gains λ_i, $i = 1, 2$ to be significantly large enough to compensate for the influence of disturbance. Similarly, in HOSMO-STC, the observer gains K_i, $(i = 1, 2, 3)$ from HOSMO (16) must be sufficiently large for disturbance estimation. Those large control/observer gains magnify the undesired chattering effects of the *sign* function, thus degrading the control performance. On the other hand, UKF-STC utilizes UKF to reconstruct system states and disturbance,

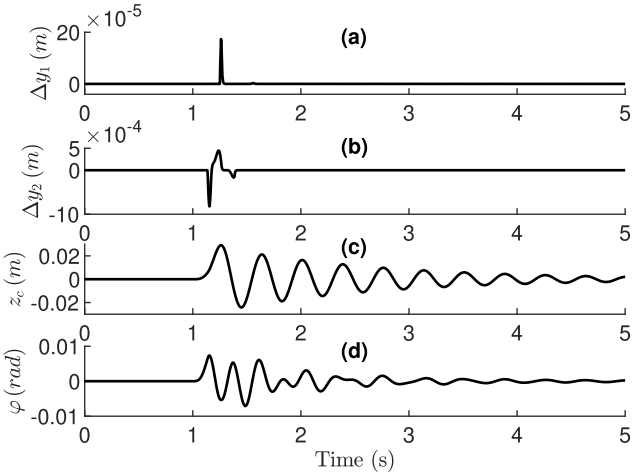

FIGURE 12. Control performance delivered by implementing FS-STC algorithm to directly stabilize the vector state of front and rear relative displacement, $X_1 = [\Delta y_1, \Delta y_2]^T$. (a) Front relative displacement. (b) Rear relative displacement. (c) Vertical displacement. (d) Pitch Angle.

then uses the estimation results for robustness enhancement in its control design. Consequently, UKF-STC offers higher accuracy, and its control gains are allowed to be relatively small, resulting in being less chattering.

Finally, the advantages and limitations of each control candidate obtained throughout the study are summarized below.

1) FS-STC:
   - Advantage: control design process is straightforward without the need for state estimation
   - Disadvantage: FS-STC requires both displacement and velocity measurements for vertical and pitch motions. Control gains associating with the *sign* function must be sufficiently large to compensate for the lumped disturbance, thus increasing the chance of chattering phenomenon.
2) HOSMO-STC:
   - Advantage: vertical and pitch velocity values are estimated, thus being less dependent on state feedback information. Control gains are consequently smaller compared with FS-STC.
   - Disadvantage: vertical and pitch displacement sensors are required. Sufficiently large observer gains must be selected to estimate disturbances, which still later leads to chattering phenomenon in control signals.
3) UKF-STC:
   - Advantage: UKF-STC does not require direct displacement and velocity measurements of vertical and pitch motions, but uses the more-practical and common relative displacement (suspension stroke) sensings. All system states can be estimated by UKF and then utilized for dynamics and disturbance compensation, thus increasing accuracy, decreasing control gains, and lowering chattering chance of happening.

- Disadvantage: Since the control design is indirect via state estimate, its performance strongly depends on UKF state estimation. Hence, careful parameter tuning is required for high precision.

V. CONCLUSION

This study tackles the problem of stabilizing a non-linear half-car suspension system while concerning about the availability of state feedback information. Three control approaches, depending on their reliance on state feedback, are proposed and compared in a task of stabilization against road profile disturbance. The comparative simulation results have shown that the proposed UKF-STC outperforms the other two controllers in terms of convergence time, accuracy, and chattering attenuation without the need for direct state feedback information. Considering the limitation of the paper, the actuator dynamics has not been considered in this study. However, the input forces F_1, F_2 obtained in this paper can be used as trajectory references for faster-dynamic controller at the lower-level loop. Another solution is to directly include the actuator dynamics in the control design, which would definitely increase the system order. For instance, hydraulic actuators are considered in [1] and [6]. In this case, mismatched disturbances, which enter the system in a different channel with the input signal, would appear in the modeling. This is reasonable as the actuator (hydraulic proportional valve) is in cascade with the plant (vehicle sprung/unsprung masses) [27]. As a result, a mismatched disturbance rejection scheme is required. This problem would be addressed in our future work.

ACKNOWLEDGMENT

The authors would like to thank Prof. K. C. Veluvolu from Kyungpook National University for the course on writing for research, which they find highly beneficial to the development and improvement of this current work.

REFERENCES

[1] W. Sun, H. Pan, and H. Gao, "Filter-based adaptive vibration control for active vehicle suspensions with electrohydraulic actuators," *IEEE Trans. Veh. Technol.*, vol. 65, no. 6, pp. 4619–4626, Jun. 2016.
[2] H. Pan, W. Sun, X. Jing, H. Gao, and J. Yao, "Adaptive tracking control for active suspension systems with non-ideal actuators," *J. Sound Vib.*, vol. 399, pp. 2–20, Jul. 2017.
[3] H. Yan, J. Sun, H. Zhang, X. Zhan, and F. Yang, "Event-triggered H_∞ state estimation of 2-DOF quarter-car suspension systems with nonhomogeneous Markov switching," *IEEE Trans. Syst., Man, Cybern., Syst.*, vol. 50, no. 9, pp. 3320–3329, Sep. 2018.
[4] H. Pang, X. Zhang, and Z. Xu, "Adaptive backstepping-based tracking control design for nonlinear active suspension system with parameter uncertainties and safety constraints," *ISA Trans.*, vol. 88, pp. 23–36, May 2019.
[5] H. Pan, X. Jing, W. Sun, and H. Gao, "A bioinspired dynamics-based adaptive tracking control for nonlinear suspension systems," *IEEE Trans. Control Syst. Technol.*, vol. 26, no. 3, pp. 903–914, May 2018.
[6] J. J. Rath, M. Defoort, H. R. Karimi, and K. C. Veluvolu, "Output feedback active suspension control with higher order terminal sliding mode," *IEEE Trans. Ind. Electron.*, vol. 64, no. 2, pp. 1392–1403, Feb. 2017.
[7] M. Papadimitrakis and A. Alexandridis, "Active vehicle suspension control using road preview model predictive control and radial basis function networks," *Appl. Soft Comput.*, vol. 120, May 2022, Art. no. 108646.
[8] A. M. Al Aela, J.-P. Kenne, and H. A. Mintsa, "Adaptive neural network and nonlinear electrohydraulic active suspension control system," *J. Vib. Control*, vol. 28, nos. 3–4, pp. 243–259, Feb. 2022.
[9] J. Na, Y. Huang, X. Wu, Y.-J. Liu, Y. Li, and G. Li, "Active suspension control of quarter-car system with experimental validation," *IEEE Trans. Syst., Man, Cybern., Syst.*, vol. 52, no. 8, pp. 4714–4726, Aug. 2022.
[10] X. Ding, R. Li, Y. Cheng, Q. Liu, and J. Liu, "Design of and research into a multiple-fuzzy PID suspension control system based on road recognition," *Processes*, vol. 9, no. 12, p. 2190, 2021.
[11] Y. Jeong, Y. Sohn, S. Chang, and S. Yim, "Coordinated compensation between active and semi-active actuators for suspension control system," *IEEE Access*, vol. 10, pp. 56207–56217, 2022.
[12] J. Wang, F. Jin, L. Zhou, and P. Li, "Implementation of model-free motion control for active suspension systems," *Mech. Syst. Signal Process.*, vol. 119, pp. 589–602, Mar. 2019.
[13] J. J. Rath, M. Defoort, C. Sentouh, H. R. Karimi, and K. C. Veluvolu, "Output-constrained robust sliding mode based nonlinear active suspension control," *IEEE Trans. Ind. Electron.*, vol. 67, no. 12, pp. 10652–10662, Dec. 2020.
[14] H. Pan and W. Sun, "Nonlinear output feedback finite-time control for vehicle active suspension systems," *IEEE Trans. Ind. Informat.*, vol. 15, no. 4, pp. 2073–2082, Apr. 2019.
[15] G. Wang, M. Chadli, and M. V. Basin, "Practical terminal sliding mode control of nonlinear uncertain active suspension systems with adaptive disturbance observer," *IEEE/ASME Trans. Mechatronics*, vol. 26, no. 2, pp. 789–797, Apr. 2020.
[16] G. Wang, C. Chen, and S. Yu, "Finite-time sliding mode tracking control for active suspension systems via extended super-twisting observer," *Proc. Inst. Mech. Eng. I, J. Syst. Control Eng.*, vol. 231, no. 6, pp. 459–470, May 2017.
[17] L. V. Meetei and D. K. Das, "Fully active suspension design using super twisting sliding mode control based on disturbance observer and ensemble Kalman filter," in *Proc. IEEE Calcutta Conf. (CALCON)*, Feb. 2020, pp. 253–257.
[18] H. Duck Choi and S. Hyun You, "Fuzzy finite memory state estimation for electro-hydraulic active suspension systems," *IEEE Access*, vol. 9, pp. 99364–99373, 2021.
[19] Z. Zhang, N. Xu, H. Chen, Z. Wang, F. Li, and X. Wang, "State observers for suspension systems with interacting multiple model unscented Kalman filter subject to Markovian switching," *Int. J. Automot. Technol.*, vol. 22, no. 6, pp. 1459–1473, 2021.
[20] H. Guo, D. Cao, H. Chen, C. Lv, H. Wang, and S. Yang, "Vehicle dynamic state estimation: State of the art schemes and perspectives," *IEEE/CAA J. Autom. Sinica*, vol. 5, no. 2, pp. 418–431, Mar. 2018.
[21] J. Davila, L. M. Fridman, and A. Levant, "Second-order sliding-mode observer for mechanical systems," *IEEE Trans. Autom. Control*, vol. 50, no. 11, pp. 1785–1789, Nov. 2005.
[22] A. Levant, "Robust exact differentiation via sliding mode technique," *Automatica*, vol. 34, no. 3, pp. 379–384, Mar. 1998.
[23] J. A. Moreno and M. Osorio, "Strict Lyapunov functions for the super-twisting algorithm," *IEEE Trans. Autom. Control*, vol. 57, no. 4, pp. 1035–1040, Apr. 2012.
[24] A. Chalanga, S. Kamal, L. M. Fridman, B. Bandyopadhyay, and J. A. Moreno, "Implementation of super-twisting control: Super-twisting and higher order sliding-mode observer-based approaches," *IEEE Trans. Ind. Electron.*, vol. 63, no. 6, pp. 3677–3685, Jun. 2016.
[25] A. Levant, "Higher-order sliding modes, differentiation and output-feedback control," *Int. J. Control*, vol. 76, nos. 9–10, pp. 924–941, Jan. 2003.
[26] R. V. D. Merwe and E. A. Wan, "The square-root unscented Kalman filter for state and parameter-estimation," in *Proc. IEEE Int. Conf. Acoust., Speech, Signal Process.*, vol. 6, May 2001, pp. 3461–3464.
[27] D. Ginoya, P. D. Shendge, and S. B. Phadke, "Sliding mode control for mismatched uncertain systems using an extended disturbance observer," *IEEE Trans. Ind. Electron.*, vol. 61, no. 4, pp. 1983–1992, Apr. 2014.

DUC GIAP NGUYEN received the B.S. degree in mechatronics from the Hanoi University of Science and Technology, Vietnam, in 2018, and the M.S. degree in mechanical and automotive engineering from the University of Ulsan, South Korea, in 2021. He is currently pursuing the Ph.D. degree in automotive engineering with Kyungpook National University. His main research interests include nonlinear control algorithm design, variable structure control, and optimization and decision-making for autonomous vehicle.

KYOUNGTAE JI (Graduate Student Member, IEEE) received the B.S. degree from the School of Mechanical Engineering, Kyungpook National University, where he is currently pursuing the master's degree. His research interests include the game theory, decision-making strategy of autonomous vehicles, and optimal path planning.

TAM W. NGUYEN (Member, IEEE) received the M.Sc. degree in mechatronics engineering and the Ph.D. degree in control systems from the Free University of Brussels, Belgium, in 2014 and 2018, respectively. He was a Postdoctoral Researcher from the Aerospace Engineering Department, University of Michigan, Ann Arbor, from 2019 to 2020. Since 2021, he has been an Assistant Professor with the Department of Electrical and Electronic Engineering, University of Toyama, Japan. His interests include nonlinear control, optimization control, and robotics.

KYOUNGSEOK HAN (Member, IEEE) received the B.S. degree in civil engineering (minor in mechanical engineering) from Hanyang University, Seoul, South Korea, in 2013, and the M.S. and Ph.D. degrees in mechanical engineering from the Korea Advanced Institute of Science and Technology (KAIST), Daejeon, South Korea, in 2015 and 2018, respectively.

He was a Research Fellow at the University of Michigan, from June 2018 to February 2020. Since March 2020, he has been an Assistant Professor with the School of Mechanical Engineering, Kyungpook National University. His current research interests include modeling and control of autonomous vehicle, energy-efficient control of electrified vehicle, autonomy, and optimization techniques.